International Symposium
On Turbulence and Shear Flow
Phenomena (TSFP-8)
August 28 - 30, 2013 Poitiers, France

EFFECTS OF ROUGHNESS ELEMENTS ON THE SEPARATION OF LAMINAR BOUNDARY LAYERS

Beratlis, N.
School for Engineering of Matter, Transport and Energy
Arizona State University
Tempe, AZ
nikos.beratlis@gmail.com

Vizard, A.
Department of Mechanical and Aerospace Engineering
The George Washington University
Washington, DC
avizard@gwu.edu

Squires, K.
School for Engineering of Matter, Transport and Energy
Arizona State University
Tempe, AZ
squires@asu.edu

Balaras, E.
Department of Mechanical and Aerospace Engineering
The George Washington University
Washington, DC
balaras@gwu.edu

ABSTRACT

A series of direct numerical simulations (DNS) of the flow past a zero pressure gradient flat plate with rows of dimples is carried out. The Reynolds number based on the boundary layer thickness is 1000 and the dimples have a circular profile with a depth to diameter ratio of 0.1. The incoming flow is laminar and the ratio of the incoming boundary layer thickness to the dimple depth determines the critical Reynolds number, where transition to turbulence occurs downstream. This happens as the shear layer that forms at the dimple edge separates over the first row of dimples and becomes unstable creating coherent vortex sheet. The vortex sheet undergoes a complex spanwise instability transforming themselves into a packet of horseshoe vortices. As a result the boundary layer downstream of the dimples has the same qualitative features encountered in wall bounded turbulent boundary layers.

INTRODUCTION

The flow of turbulent boundary layers over rough walls has been extensively studied both experimentally and numerically due to its significance in a variety of applications ranging from engineering to geophysics (see Jimenez 2004 for a review). The flow of laminar boundary layers over rough walls, on the other hand, has not received the same level of attention, although there is a wide range of potential applications primarily in separation control. A great example is that of golf balls, where dimples are used to reduce the drag force by as much as 50% when compared to a smooth sphere at the same Reynolds number. It is generally accepted that dimples cause the laminar boundary layers to transition to turbulence, energizing the near wall flow and adding momentum, which helps overcome the adverse pressure gradient and delay separation. Recently Choi *et al.* (2011) carried out a series of experiments on dimpled spheres to clarify the mechanism of drag reduction caused by dimples. Using hot-wire anemometry they measured the streamwise velocity within individual dimples and showed that the boundary layer separates locally within the dimples. They concluded that turbulence is generated by a shear layer instability which causes momentum transfer of high speed fluid towards the surface of the sphere. Further support for this mechanism was provided by recent direct numerical simulations (DNS) by Smith *et al.* (2010). In their work, flow visualization identified the formation of thin shear layers at the leading edge of the dimples, which become unstable and are effective in energizing the near-wall flow. The

detailed mechanics of delaying the separation of the boundary layer and the role of the type and topology of the type and arrangement of the dimples is still not well understood.

Experimentally there are inherent difficulties of measuring flow quantities near and within the dimples, while numerically it becomes prohibitively expensive to accurately resolve high Reynolds number flow over dimpled spheres. In the present study we will report Direct Numerical Simulations (DNS) of the flow past a flat plate with rows of circular dimples. This way we can isolate some of the fundamental phenomena present in such flows and at the same time keep the cost of the computations low in order to explore a wide parametric range. We will investigate how dimples cause transition to turbulence and quantify the nature of the boundary layer in the post-dimple area by direct comparison with equilibrium wall bounded turbulent flows. In the following sections the problem setup and methodologies will be presented, followed by the results and conclusions sections.

PROBLEM SETUP

Figure 1a shows an outline of one of the geometries used in this study. It consists of a flat plate upon which one row of circular dimples is placed at some distance downstream of a laminar boundary layer. The dimple has a maximum depth d and a circumscribed diameter D. The ratio d/D in this particular case is set to 0.1 which is representative of that found on today's golf balls. The effect of a second row of dimples and its alignment with respect to the first one was also investigated. The corresponding geometries are shown in figure 1b and c. In one case the second row of dimples is aligned with the first one while in the another case the second row of dimples forms a staggered arrangement.

For all cases the domain is centered on the first row of dimples and extends $0.55D$ upstream of the leading edge of the first row of dimples and $5D$ downstream of the trailing edge of the last row of dimples. The top boundary is located at $1.9D$ above the flat plate. At the inlet the velocity profile obtained from the the Blasius solution is specified. This enables to control the height of the boundary layer so that that the desired ratio δ/d is achieved at the leading edge of the first row of dimples. At the top boundary the wall normal velocity component obtained from the Blasius solution is specified. This type of boundary condition provides the correct mass flux through the top boundary to account for the Blasius boundary layer growth. It becomes less accurate in our case due to the presence of the dimple and the fact that the flow downstream of the dimples is not laminar. However, it doesn't result in a significant free-stream acceleration, and the value of the acceleration parameter, $K = -(\nu/U_\infty^2)(dU_\infty/dz)$ (where ν is the kinematic viscosity of the fluid, U_∞ is the freestream velocity and z is the coordinate in the streamwise direction) never exceeded $K = 3.5 \times 10^{-8}$. This is fairly low value and it is not expected that the acceleration plays a significant role on either the transition mechanics at the dimple level or on the formation of turbulent-like structures in the post-dimple region. At the outlet a convective boundary condition was used while a periodic boundary condition is used in the spanwise direction.

The governing equations for a viscous incompressible flow are discretized on a structured grid in Cartesian coordinates. The geometry of the dimpled flat plate, which is not aligned with the grid lines, is treated using an immersed-boundary formulation (see Balaras 2004 and Yang & Balaras 2006). An exact, semi-implicit, projection method is used for the time advancement. All terms are treated explicitly using the Runge-Kutta 3rd order scheme, except for the viscous and convective terms in the wall normal direction which are treated implicitly using the 2nd order Crank-Nicholson scheme. All spatial derivatives are discretized using second-order central-differences on a staggered grid. The code is parallelized using a domain decomposition approach, where the computational box is evenly divided along the stream wise direction and communication between processors is done using MPI library calls.

The computational grid, which is designed to resolve both the shear layer dynamics within the dimple, as well as, the boundary layer that forms downstream of the dimples is stretched in the wall normal and streamwise directions. In particular in the post-dimple region the grid spacing are $\Delta x^+_{min} = 0.009$ for the first cell away from the flat plate, uniform $\Delta y^+ = 6.5$ and $\Delta z^+_{max} = 11$, where x, y and z are the wall normal, spanwise and streamwise directions respectively. In the dimples there are 90 points across its maximum depth, 120 points in the streamwise direction between the trailing and leading edges of the dimples and 220 points across its diameter in the spanwise direction. Therefore the fine grid employed in this study is adequate to resolve the important features of the flow. In total there are $394\times452\times752$ grid points in the wall-normal, spanwise and streamwise directions respectively for the case of one row of dimples and $394\times452\times852$ grid points for the case of two rows of dimples.

The simulations were initialized with the Blasius solution and probes were placed in the flow to monitor the evolution of the transient state. It was found that after approximately $200D/U$ time units the flow reached a periodic state. After time $400D/U$ the flow was sampled and time-averaged statistics were calculated for a period of $500D/U$ time units.

RESULTS

Given the circular dimple geometry the important dimensionless parameters that control transition from a laminar to turbulence state in the post-dimple region are: i) the ratio $\alpha = \delta/d$ of the boundary layer thickness, δ, at the leading edge of the dimple to the dimple depth d; ii) the Reynolds number, $Re_\delta = U\delta/\nu$, based on the freestream velocity, U, the kinematic viscosity, ν, and δ. We conducted a series of computations where we systematically varied α and Re and constructed a stability map for the case of one and two rows of dimples aligned. For each simulation the flow downstream of the dimples was monitored and based on the behavior of the skin friction coefficient, C_f, downstream of the dimple center the flow was characterized. In particular, if C_f in the post-dimple area dropped to values reminiscent of a laminar boundary layer then the dimples were not successful in destabilizing the boundary layer and thus the flow is characterized as stable. On the contrary if C_f deviated from laminar values and exhibited strong fluctuations then the dimples were successful in destabilizing the boundary layer and the flow was characterized as unstable. Figure 2 shows the stability map for the cases of one row of dimples and two rows of dimples aligned. The critical Reynolds number Re_{cr} is the threshold at which transition to a non-laminar flow down-

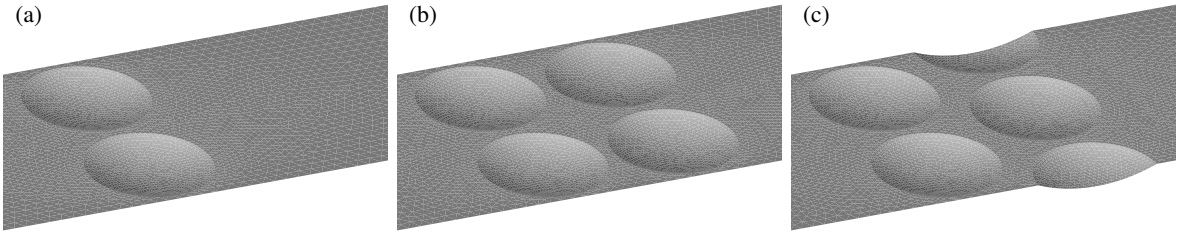

Figure 1. Geometries of a flat plate with various roughness elements used in this study a) one row of dimples b) two rows of dimples aligned and c) two rows of dimples staggered.

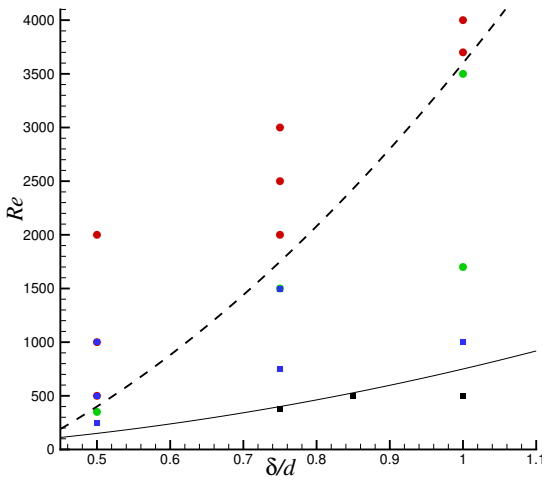

Figure 2. $Re-\delta/d$ stability map for the flat plate with dimples. – – – stability boundary for one row of dimples; ——— stability boundary for two rows of dimples aligned. Region below the line is stable and above the line is unstable

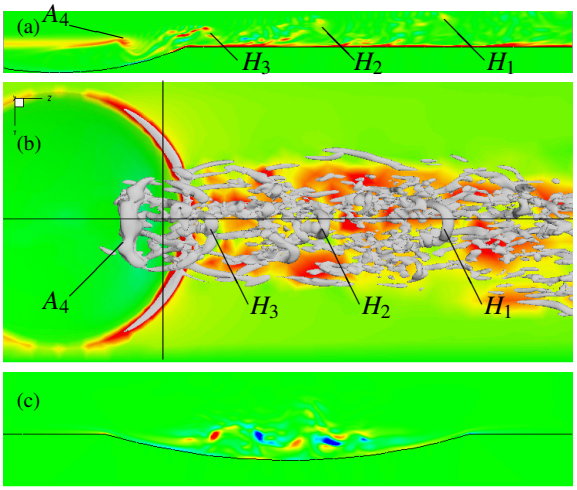

Figure 3. a) Contours of spanwise vorticity ω_y on a vertical $x-z$ plane passing through the center of the dimple. b) Isosurface of the Q criterion and contours of C_f on the wall. c) Contours of streamwise vorticity ω_z on a vertical $x-y$ plane located just downstream of vortical structure A_4.

stream of the dimple is observed. For a fixed δ/d transition occurs at any $Re_\delta > Re_{cr}$ while below Re_{cr} the flow remains laminar. For a zero pressure gradient smooth flat plate Re_{cr} ~4000. It is obvious that even a single row of dimples has a drastic effect in lower the critical Reynolds number. For $\delta/d = 1$ Re_{cr} ~3500, a little lower than that for a smooth flat plate. As δ/d decreases (the boundary layer becomes thinner compared to the dimple depth) Re_{cr} decreases at a non-linear fashion. When a second row of dimples is added Re_{cr} is decreased significantly. The decrease in Re_{cr} is more pronounced at higher values of δ/d, where at $\delta/d = 1$ Re_{cr} for the case of two rows of dimples is about 6 times lower than that for one row.

The origin of this instability can be better understood by looking at the instantaneous flow structures. For all the cases presented in this paper $Re_\delta = 1000$ and $\delta/d = 0.5$. Figure 3 shows a snapshot of the spanwise vorticity on a spanwise (x-z) plane passing through the center of one of the dimples accompanied by isosurfaces of the Q criterion viewed from above. The time corresponds to an instant when the shear layer forming over the dimple starts to roll-up into a vortical structure A_4. The roll-up occurs at a point between the center and the trailing edge of the dimple. Vortical structure A_4 which is still coherent doesn't span across the entire dimple. As one moves towards the edges of the dimple in the spanwise direction the dimple becomes more shallow and a roll-up is suppressed. As a result the spanwise length of vortical structure A_4 is approximately 1/3 that of the dimple diameter D. It is important to note that vortical structure A_4 is not uniform in the span and consists of bends and kinks. Just downstream of vortical structure A_4 there are a pair of vortices elongated in the streamwise direction and slanted upwards reminiscent of braid vortices found in free shear layers. A plot of contours of the streamwise vorticity ω_z on a vertical $x-y$ plane slicing through the legs of these vortices is shown in figure 3c. The plot reveals that the flow inside the dimple is three dimensional consisting of two pairs of counter rotating vortices. The braid vortices form the legs of a hairpin like vortex whose head is clearly identified as structure H_3 in figure 3b. The heads of two more hairpin like vortices H_2 and H_1 can be seen further downstream in the post-dimple area separated by each other by approximately $0.6D$.

The evolution of vortical structure A_4 plays a key role in the formation of hairpin like vortices and the transition in the post-dimple region. The small bends and kinks present in vortical structure A_4 are subjected to local shear resulting into the formation of a Λ type vortex consisting of a head H_4 and a pair of legs L_4. As this structure propagates further in the post-dimple region it evolves into a hairpin like vortex whose head H_4 is shown at a later time in figure 4. The heads H_2 and H_3 of previously formed hairpin like structures can also be seen as far as 1.5D diameters downstream of the trailing edge of the dimple. Their lifetime is therefore at least $20D/U$ time units. The above instantaneous dynamics suggest that the spanwise vorticity ω_y present in the shear layer transforms into streamwise

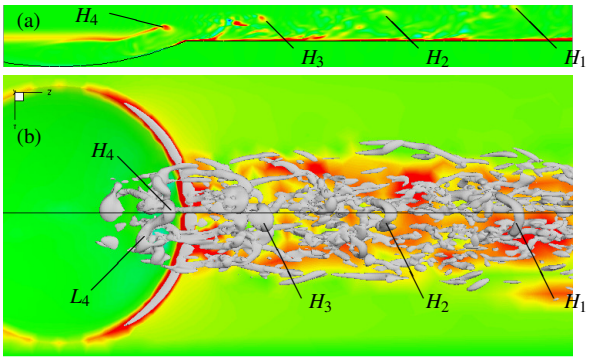

Figure 4. a) Contours of spanwise vorticity ω_y on a vertical plane passing through the center of the dimple and b) isosurface of the Q criterion and contours of C_f on the wall.

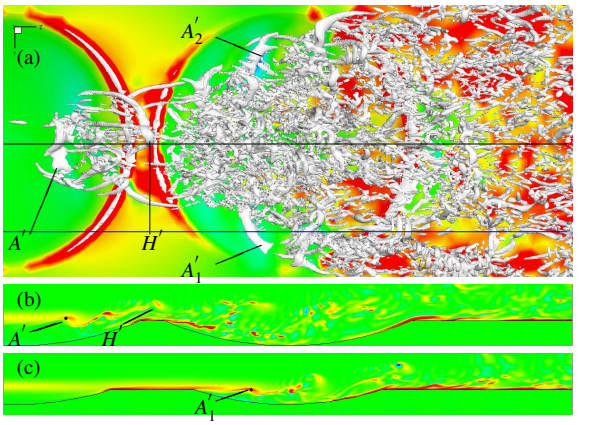

Figure 5. a)Isosurface of the Q criterion and contours of C_f on the wall for the case of two rows of dimples aligned. b) Contours of spanwise vorticity ω_y on a vertical plane corresponding to horizontal black line in (a). c) Contours of spanwise vorticity ω_y on a vertical plane corresponding to horizontal blue line in (a).

vorticity ω_z through a Λ type instability. With each vortex shed from the shear layer a hairpin like vortex forms in the midplane of the dimple and a packet of streamwise vortical structures located behind, and to the sides of the hairpin. As these streamwise vortices travel downstream they generate new hairpin vortices and the turbulent front appears to grow in the spanwise direction and generating more streamwise oriented vortices. The metamorphosis of a hairpin vortex into a turbulent spot and its organization in wall turbulence has been previously studied and are well documented by Adrian (2007) and Singer & Joslin (1994).

For the case of two rows of dimples that are aligned, the instantaneous flow structures as visualized by the Q criterion and are shown in Figure 5. Over the first dimple the flow dynamics are very similar to those observed for a single row of dimples. Namely the shear layer becomes unstable and rolls-up into a coherent structure A' containing mainly azimuthal vorticity. This coherent structure undergoes three dimensional instabilities transforming itself into a packet of hairpin-like vortices. One such hairpin-like vortex resulting from the transformation of a previous roll-up is clearly identified in figure 5 and labeled as H'. Other hairpin-like structures are visible behind and to the sides of H'.

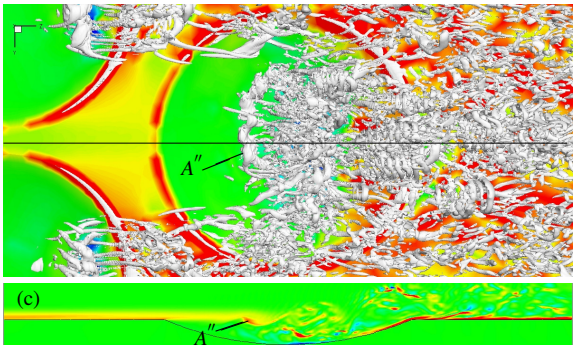

Figure 6. a)Isosurface of the Q criterion and contours of C_f on the wall for the case of two rows of dimples staggered. b) Contours of spanwise vorticity ω_y on a vertical plane corresponding to horizontal black line in (a).

The flow dynamics over the second row of dimples are quite different. First, there is no coherent roll-up of the shear layer at the center of the dimple as is evident in the first row. A thin shear layer appears in the contours of spanwise vorticity at the mid-plane of the dimple but it is not coherent in the spanwise direction and it appears to break down quickly. The dominant structures over the second dimple consist of the packet of hairpin-like structures originating from the first row of dimples. As this packet propagates over the dimple it generates other streamwise oriented vortices before it eventually breaks down. Contrary to the case of the single row where hairpin-like vortices originating from the shear layer could be traced at least two diameters downstream of the trailing edge of the dimple, hairpin-like vortices appear to breakdown within the second row of dimples.

Another important difference in the flow dynamics within the second row of dimples is that closer to the sides of the dimples the shear layer becomes unstable and rolls-up into coherent vortical structures. These structures labeled A_1'' and A_2'' are located on both sides of the dimple and appear slightly bent in the spanwise direction. Visualization of the flow field at different times reveals that structures A_1'' and A_2'' undergo three dimensional instabilities that give birth to new hairpin-like vortices. The effect of the roll-up over the second dimple on the spanwise extend of the turbulent-like structures is dramatic. In particular the hairpin-like vortices forming on the sides of the second row of dimples along with those evolving from the center of the first row of dimples fill up the entire spanwise domain already by the trailing edge of the dimple.

Figure 6 shows an isosurface of the Q critetion for the case of two rows of dimples staggered. Contours of spanwise vorticity are also shown at a spanwise plane passing through the center of the second row of dimples. Over the first row of dimples the shear layer instability is the same as that for a single row of dimples. In particular, the coherent structure resulting form the roll-up of the shear layer undegoes three-dimensional instabilities transforming itself into a packet of hairpin-like vortices. The dynamics of the shear layer in the second row are very similar too with a coherent structure seen in the center of the dimple and spanning about one third of the dimple diameter. The vortical structure labeled A'' undergoes a Λ type instability. When the hairpin-like structures originating from the first row of dimples pass over the sides of the second row of dimple they merge with the hairpin-like structures of the second row of

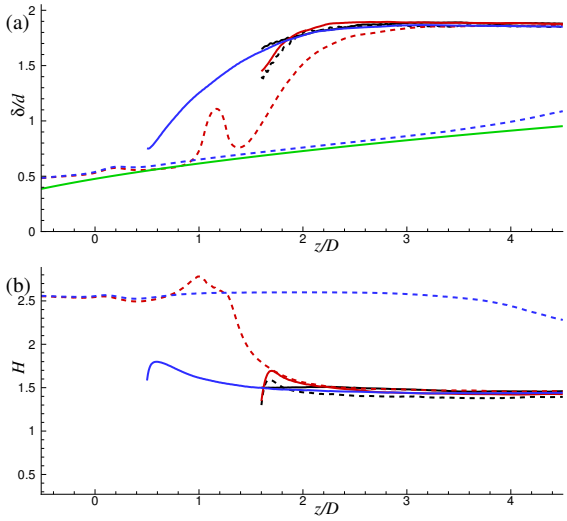

Figure 7. a) Boundary layer thickness δ/d and b) shape factor H versus streamwise coordinate z/D at two spanwise locations, one passing through the center of the dimples in the first row (solid lines) and one passing between the dimples in the first row (dashed line). Colors rerpesent: ——; 1 row of dimples, ——; 2 rows aligned, ——; 2 rows staggered, ——; Blasius laminar boundary layer.

dimples. As a result a front of turbulent-like structures fills the entire span of the domain before the trailing edge of the second row of dimples.

Next we look at the effect that the hairpin-like structures have on the dynamics of the post-dimple boundary layer. Figure 7a shows the evolution of the boundary layer thickness, δ, as a function of z at two spanwise locations; one passing through the center of the dimples in the first row and one passing between the dimples in the first row. When these lines pass through the dimples δ is not plotted since the flow in the dimples separates and the boundary layer thickness is not clearly defined there. For reference the thickness for the Blasius laminar boundary layer (i.e. how δ would evolve in the absence of dimples) is also plotted in the figure. For the case of one row of dimples δ before the leading edge and between the dimples grows very similarly to that of the Blasius solution indicating that the flow is mostly laminar. Only after $z/D \sim 4$ does δ deviate from the laminar solution and starts to grow a little faster. A different behavior is evident downstream of the dimple center, δ immediately after the trailing edge of the dimple grows very rapidly and reaches an asymptotic value of $1.85d$ around $z/D \sim 2.5$. For the cases of two rows of dimples δ also grows very quickly everywhere along the span and deviates significantly from the Blasius solution. At $z/D = 3$ δ becomes uniform across the span and attains a value of $1.85d$. The shape factor H behaves in a similar way, for the case of one row of dimples and for a line passing between the dimples H remains at 2.5 during most of the post-dimple area and slightly decreases after $z/D \sim 3.5$. For all other cases H decreases rapidly and already by $z/D = 2$ it reaches a value of value of 1.45 reminiscent of turbulent wall bounded flows. This behaviour indicates that for the case of two rows of dimples transition downstream of the dimples takes place very quickly at different spanwise locations. For the case of one row of dimples the transition is confined to a region downstream of the dimple center while between the dimples the flow remains laminar.

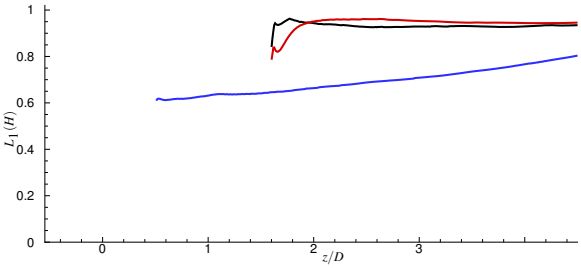

Figure 8. L_1 norm of the shape factor H as defined by equation 1. —— 1 row of dimples; —— 2 rows aligned; —— 2 rows staggered.

From the above discussion it is obvious that the flow can differ dramatically along the span downstream of the dimple. In the region between the dimples the flow remains laminar for at least three dimple diameters while the flow downstream of the dimple center quickly tends towards an equilibrium state of wall turbulence. It is therefore reasonable to ask how the flow behaves between these two spanwise planes and try to quantify the growth of the turbulent activity in the spanwise direction. In order to quantify the spanwise mixing the L_n norms of the shape factor H were calculated as follows:

$$L_n(H(z)) = \left[\frac{1}{L_y}\int_0^{L_y} \frac{|H_{lam} - H|^n}{(H_{lam} - H|_{min,y})^n} dy\right]^{1/n} \quad (1)$$

where L_y is the spanwise length of the domain, H_{lam} is the value of the shape factor for a laminar boundary layer and $H|_{min,y}$ is the minimum value of H across the span at a given z. When the flow is turbulent across the entire span $L_n(H)$ attains a value of 1, whereas values less than 1 indicate that turbulent activity extends to only a part of the spanwise domain. Figure 8 shows $L_1(H)$ as a function of streamwise coordinate z for all three cases. For the case of only one row of dimples $L_1(H)$ at the trailing edge of the dimples is about 0.5, that is the front of turbulent structures cover only half of the domain in the span. As one moves downstream $L_1(H)$ grows in an almost linear fashion however even at $z/D = 4.5$ $L_1(H)$ reaches a value of 0.78 which means that the turbulent activity at four dimple diameter downstream doesn't fill the entire span. For the cases of two rows of dimples $L_1(H)$ is already 0.8 at the trailing edge of the second row of dimples. In the case of the staggered alignment the spanwise growth appears to be a little faster although in both cases $L_1(H)$ reaches values of approximately 0.95 within half a dimple diameter. The above results suggests that the addition of a second row of dimples in either aligned or staggered arrangement has an important effect in accelerating the spanwise growth of turbulent activity in the post-dimple boundary layer.

Figure 9 shows average velocity profile and rms of the velocity at $z/D = 4.5$. For the case of one row of dimples the spanwise location corresponds to the location of the dimple center while for the cases of two rows of dimple the profiles have been ensemble avaraged in the span since the flow is practically homogeneous at that downstream location. For comparison the corresponding rms profiles for a zero pressure gradient turbulent boundary layer by Wu & Moin (2009) are also plotted. The velocity profiles plotted in wall coordinates for all cases exhibit a log law in the

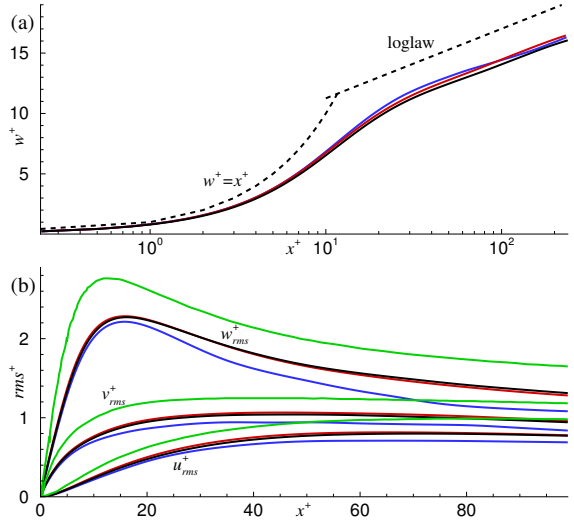

Figure 9. a) Profile of average streamwise velocity and b) rms velocity fluctuations. —— 1 row of dimples; —— 2 rows aligned; —— 2 rows staggered; —— zero pressure gradient turbulent boundary layer DNS results by Wu & Moin (2009).

outer region albeit the values are underestimated. This shift is an artifact of the very low Reynolds numbers which results in higher values of the skin friction coefficient C_f. A similar behaviour is evident in the rms of the velocity fluctuations. Although the rms profiles exhibit the same qualitative behaviour as those for a zero pressure gradient turbulent boundary layer with peaks near the wall the values are underestimated.

CONCLUSIONS

A series of direct numerical simulations of the flow over a flat plate with one and two rows of dimples has been carried out. A stability map as a function of the incoming Reynolds number and ratio of boundary layer thickness, δ, to the dimple depth, d, was constructed. We found that the addition of the second row of dimples dramatically decreases the critical Reynolds number where transition occurs in the downstream area. The initial disturbances are generated as the shear layer that forms over the first raw of dimples becomes unstable and roll-ups into a coherent vortex sheet containing mainly spanwise vorticity. The vortex sheet undergoes a spanwise instability generating horseshoe-like vortices with a strong streamwise vorticity component. These structures propagate into the post-dimple boundary layer and are effective in sustaining *equilibrium*, low Reynolds number, turbulence. In particular, the shape factor, H, drops to value of 1.45, which is reminiscent of turbulent wall bounded flows, just within one dimple diameter downstream of the trailing edge of the dimples. For the case of one row of dimples this turbulent-like activity is confined to a narrow strip downstream of the dimple center and grows slowly in the spanwise direction as the boundary layer grows. The addition of a second row of dimples amplifies the spanwise growth of turbulence and already by the end of the second row turbulent-like structures fill the entire span of the domain.

ACKNOWLEDGEMENTS

EB and AV where partially supported by the National Science Foundation Grand CBET-0933642. This work used the Saguaro high-performance computer cluster at ASU's Advanced Computing Center, and the Extreme Science and Engineering Discovery Environment, XSEDE (award TG-CTS110028).

REFERENCES

Adrian, Ronald J 2007 Hairpin vortex organization in wall turbulence. *Physics Of Fluids* **19** (4), 041301.

Balaras, E 2004 Modeling complex boundaries using an external force field on fixed Cartesian grids in large-eddy simulations. *Computers and Fluids* **33** (3), 375–404.

Choi, J, Jeon, WP & Choi, H 2011 Mechanism of drag reduction by a surface trip wire on a sphere . *Journal of Fluid ...* **672**, 411–427.

Jimenez, J 2004 Turbulent flows over rough walls. *Annual Review Of Fluid Mechanics* **36**, 173–196.

Singer, Bart A & Joslin, Ronald D 1994 Metamorphosis of a hairpin vortex into a young turbulent spot. *Physics Of Fluids* **6** (11), 3724–3736.

Smith, C E, Beratlis, N, Balaras, E, Squires, K & Tsunoda, M 2010 Numerical investigation of the flow over a golf ball in the subcritical and supercritical regimes. *International Journal Of Heat And Fluid Flow* **31** (3), 262–273.

Wu, Xiaohua & Moin, Parviz 2009 Direct numerical simulation of turbulence in a nominally zero-pressure-gradient flat-plate boundary layer. *Journal Of Fluid Mechanics* **630**, 5.

Yang, JM & Balaras, E 2006 An embedded-boundary formulation for large-eddy simulation of turbulent flows interacting with moving boundaries. *Journal of Computational Physics* **215** (1), 12–40.